Spectroscopic properties of oxygen vacancies in monoclinic HfO_2 calculated with periodic and embedded cluster density functional theory

D. Muñoz Ramo, J. L. Gavartin, and A. L. Shluger
Department of Physics and Astronomy, University College London, Gower Street, London WC1E 6BT, United Kingdom
and London Centre for Nanotechnology, 17-19 Gordon Street, London WC1H 0AH, United Kingdom

G. Bersuker
SEMATECH, 2706 Metropolis Drive, Austin, Texas 78741, USA

(Received 22 December 2006; revised manuscript received 28 February 2007; published 24 May 2007)

We have calculated the electronic structure and spectroscopic properties of the oxygen vacancy in different charge states in the monoclinic phase of HfO_2. Periodic and embedded cluster calculations using density functional theory and a hybrid density functional reproduce the band gap of this material with good accuracy and predict the positions of the one-electron energy levels corresponding to five charge states of the vacancy in the band gap. The optical transition energies as well as optical and thermal ionization energies into the conduction band for all vacancy charge states and the g tensor for electron spin resonance (ESR) active states are calculated. We discuss the relation of the calculated properties to metrology of vacancies using spectroscopic ellipsometry, ESR, and electrical stress measurements.

DOI: 10.1103/PhysRevB.75.205336 PACS number(s): 61.72.Bb, 61.72.Ji, 71.20.−b, 71.15.Mb

I. INTRODUCTION

Hafnium dioxide is currently being intensively investigated primarily for its prospective application as a gate dielectric in metal-oxide-semiconductor field-effect transistors (MOSFETs). Its potential advantage over the currently used silica is in a higher static dielectric permittivity (high k) [22–25 versus 3.9 in SiO_2 (Ref. 1)], which provides a higher capacitance density for the same physical gate thickness. Recent advances in film deposition techniques dramatically improved the quality of hafnia films with respect to film density, thermal and electrical stability, as well as quality of the interface with both the silicon substrate and metal gate. However, the perfomance of prototype high-k MOSFETs is still limited by large concentrations of electron traps, leading to reduced channel carrier mobility, high value and instability of threshold potential, V_{th}, and other reliability issues.

Oxygen vacancies and interstitial ions are often implicated in causing these problems. However, to our best knowledge, no measurements have been reported that unambiguously identify specific defects. For example, Takeuchi *et al.*[2] performed laser ellipsometry of HfO_2 films of physical thickness of about 10 nm. They estimated the optical energy gap E_g at 5.7 eV and identified an additional broad absorption band at 4.5–5.0 eV. The latter has been assigned to oxygen vacancy and interpreted as an electron transition between the valence-band maximum (VBM) and the vacancy state. Both the intensity and width of the observed defect band were shown to decrease with the increase of the temperature of oxygen anneal. The authors also conducted electrical (voltage-capacitance) measurements on similar (but not identical) samples and established that the trap density also decreases with the increase of the anneal temperature. In contrast, more recent laser ellipsometry experiments by Nguyen *et al.*[3] detected an absorption band centered much closer to the optical band-gap energy, only 0.2–0.3 eV below the optical band gap (see, however, Ref. 4). All the films in that study were fabricated using either atomic layer deposition or metal-organic chemical vapor deposition. Shallow defect levels were found only in crystalline films and not observed in amorphous films.

Some defect states in HfO_2 gate stacks were also identified by electron spin resonance (ESR) measurements. As-deposited films generally show only weak paramagnetism. However, ultraviolet (UV) irradiation and electrical stress induce a strong paramagnetic signal with g-tensor parameters similar to those attributed to P_b and E' center in the Si/SiO_2 stack.[5–8] Although the intensity of the corresponding signal strongly depends on the film deposition process, in similar films it was found to be independent of film thickness and thus has been attributed to either Si/HfO_2 or Si/SiO_2 interface states. The interface ESR signal intensity has been found to correlate with the interface trap density recovered from the gate voltage-capacitance measurements.[7–12]

In contrast to the apparent consensus attributing paramagnetic defects at the interfacial Si/SiO_2 layer to P_b and E' centers, determining the origin of paramagnetic signals in the bulk of HfO_2 samples proved to be more difficult. In particular, Lenahan and co-workers[8,13] reported two groups of signals in the as-deposited samples upon electron injection. The first group is characterized by g factors of 2.04, 2.01, and 2.000 for g_{zz}, g_{yy}, and g_{xx}, respectively, and the second, less characterized signal has $g=1.965$. The observed signals were tentatively attributed to, respectively, the interstitial O_2^- ion and to Hf^{3+} ion or oxygen vacancy. Similar ESR signals have also been observed in the monoclinic HfO_2 powders,[14] but the identity of the corresponding paramagnetic centers still remains unclear. In particular, their extrinsic origin, such as Zr^{3+} or Ti^{3+} ions substituting for Hf^{4+}, could not be ruled out. We also note that no other spectroscopic properties of the paramagnetic defects discussed above have been measured simultaneously and correlated with ESR.

Finally, a third group of measurements probing electrically active states in HfO_2 films is based on charge injection into a bulk film and subsequent monitoring of the kinetics of electron trapping and detrapping to and/or from the bulk

traps. The latter is manifested in the time dependence of the shift of the threshold potential, δV_{th}.[15–18] These measurements indicate the existence of shallow electron traps characterized by thermal detrapping energies into the conduction band of around 0.3–0.5 eV, and of deeper traps, whose energies have not been properly established. The shallow traps have been attributed to two negatively charged states of the oxygen vacancy.[19,20] One should note that fast transient electrical measurements discussed here probe only those defects that are confined within a thin layer inside the oxide film. The geometrical position of this layer with respect to the gate depends on the stress voltage and is hard to determine quantitatively.

Although oxygen vacancies could be involved in the processes discussed above, this attribution remains speculative and no direct correlation between the bulk electron trap concentration and vacancy concentration has been established. Lack of unambiguous vacancy characterization precludes the development of effective ways of controlling the trap density, and theoretical modeling can help establish robust methods of vacancy identification by predicting its spectroscopic characteristics. Toward this goal, we present the results of density functional calculations of optical absorption, optical and thermal ionization energies, and g-tensor parameters of the oxygen vacancy in the monoclinic (m)-HfO_2 using a nonlocal exchange functional.

Early *ab initio* calculations of oxygen vacancy in HfO_2 and ZrO_2 mostly focused on predicting the ground-state properties and used local [local-density approximation (LDA)] or semilocal [generalized gradient approximation (GGA)] approximations with plane waves within the density functional theory (DFT) (see Refs. 21 and 22 for a review). These approximations tend to significantly underestimate single-particle band gaps. As a consequence, the position of defect levels with respect to the band edges could not be accurately determined. In addition, reliable description of shallow defect states is also problematic using these methods.[22–24] Most of these early calculations (except, perhaps, Ref. 25) considered only positively charged and neutral, i.e., V^{2+}, V^{+}, and V^{0}, vacancy states. Although the single-particle levels for these states are method dependent, most calculations agreed that positive and neutral vacancies produce deep defect states and do not fit a description of shallow electron states observed in electrical[15–18] and optical experiments.[2,3] More recently, Shen *et al.*[25] and Bersuker *et al.*[26] suggested negative oxygen vacancy states as possible shallow traps, but these semilocal calculations severely underestimated the energy split of the corresponding defect levels from the conduction-band edge. Significant improvement has been achieved by Robertson and co-workers,[21,27–29] who used screened exchange approximation to predict vacancy energy levels including V^{-} and V^{2-} charge states. However, these calculations were performed using a small periodic supercell and therefore corresponded to extremely high vacancy concentrations. Besides, the quality of the functional used in these calculations is untested and needs independent validation. Finally, none of the techniques used to perform the above calculations is capable of reliably predicting defect spectroscopic properties.

Recently, we reported calculations of oxygen vacancy in m-HfO_2 with a density functional with nonlocal exchange and a large supercell,[20] which described five vacancy charge states in terms of their conformation and single-particle electronic spectra. Based on these calculations, we estimated thermal activation energies of the negative vacancies and found them in reasonable agreement with the energies of shallow electron traps observed in transient electric measurements.[15–18] However, further identification of oxygen vacancies also requires establishing their ESR and optical spectroscopic parameters. Therefore, in this paper, we use a combined approach, whereupon we calculate the band structure of m-HfO_2 using the same periodic DFT method as in Ref. 20 and investigate optical transitions and g tensor by means of an embedded cluster approach and the same nonlocal exchange density functional.

The rest of the paper is organized as follows. In the next section, we describe the computational methods employed in this study. The results of calculations are presented in Sec. III. A discussion of the obtained data in relation to other computational methods and the reliability of one-electron level spectrum as an approximation to the study of properties discussed in this paper is presented in Sec. IV.

II. CALCULATION PROCEDURE

Bulk hafnia at atmospheric pressure and low temperature has monoclinic symmetry (space group $P2_1/c$). At $T=2000$ K, it undergoes martensitic phase transformation into the tetragonal phase (space symmetry $P4_2/nmc$), and above $T=2870$ K, the cubic fluorite structure is most stable (space symmetry $Fm3m$). The monoclinic structure is characterized by the two nonequivalent anion sublattices. In one, oxygen ions are fourfold coordinated, and in the other, they are threefold coordinated. The equilibrium O-Hf distances range between 2.14 and 2.24 Å in the former and between 2.05 and 2.14 Å in the latter sublattice. These structural parameters are well reproduced using the semilocal DFT methods[22] as well as the method described below.

Two complementary implementations of DFT, periodic and embedded cluster methods, have been used. Periodic DFT calculations were performed with a massively parallel version of the CRYSTAL03 package.[30] This method makes use of local basis sets of Gaussian-type orbitals (GTOs) and consistently demonstrates good performance in studying the electronic structure of a broad class of insulators.[31,32] We use an all-electron basis set on oxygen ions, which has been used previously to study a wide range of oxides,[33] with the outer exponents optimized for better description of m-HfO_2. It includes 14s, 6p, and 1d functions contracted to 1s and 3sp shells using an 8/411/1 scheme. A similar basis set was also centered at the vacant oxygen site when calculating the oxygen vacancy. For hafnium atoms, we used a small relativistic effective core potential (RECP) introduced by Stevens *et al.*[34] and adapted for the CRYSTAL code. Twelve outer electrons are considered explicitly, while the core electrons and the nucleus are substituted by an effective core pseudopotential. The basis set consists of 6s, 6p, and 4d functions contracted to 3sp and 2d shells using a 411/31 scheme.

The characteristics of the oxygen vacancy in m-HfO_2 were calculated using a 95-atom supercell. This setting offers

a good compromise between achieving a large separation of charged vacancies and computational effort related to the number of atoms and basis functions in the cell. The vacancy was located in a four-coordinated site, as previous studies have shown that negatively charged vacancies are more stable in this site rather than in the three-coordinated one.[22,35] However, the one-electron spectrum does not show significant changes with respect to the choice of coordination site.

The integration in reciprocal space has been carried out on a Monkhorst-Pack mesh of 36 k points in the irreducible part of the Brillouin zone. The numerical accuracy thresholds used to ensure convergence of the self-consistent field procedure were set to 10^{-5} eV for the one-electron eigenvalues and 10^{-6} eV for the total energy. A uniform charge background was used in calculations of charged vacancies. The geometry optimization was performed for each charge state of the vacancy, with the tolerances set to 0.0005 a.u. $Å^{-1}$, 0.0003 a.u. $Å^{-1}$, 0.002 Å, and 0.001 Å for the maximum gradient, average gradient, maximum displacement, and average displacement, respectively.

The calculations were performed using the hybrid B3LYP exchange-correlation functional, which combines a parametric combination of the Hartree-Fock and local exchange due to Becke (B3) and the correlation functional of Lee, Young, and Parr (LYP).[36,37] Although no solids or transition-metal compounds have been used in the parameter fitting for the exchange potential, there is a general consensus that this functional gives good description of structure and other properties of simple and magnetic oxides and their surfaces,[31,32,38–40] and of perovskites,[32] and in determining band gaps in these and other materials.[41] The latter property is particularly important for obtaining reliable results in this study.

Calculations in the periodic model allow one to determine the geometric structure of oxygen vacancy in different charge states as well as its thermal ionization energies with respect to the bottom of the conduction band.[20] However, optical absorption and ESR properties are more readily calculated within molecular quantum-chemical methods. To study defects in insulators, the molecular model can be improved by taking into account the interaction of the quantum cluster including a defect and neighboring ions with the rest of the host lattice, the perturbation of the lattice by the defect, and the reciprocal effect of the lattice polarization on the defect itself. This is achieved by constructing an external potential in which the cluster is then embedded and by surrounding the cluster by an infinite polarizable lattice treated using the classical force field approach. Such a potential is called an embedding potential, and the model, the embedded cluster model. Accurate representation of the embedding potential is a major challenge, with several approaches existing (see, for example, Refs. 42–44 for recent reviews).

Here we use a simplified approach, where a quantum cluster including the vacancy and its vicinity (pictured in Fig. 1) is embedded in the rest of the crystal represented by a lattice of classical rigid ions. First, using a 96-atom unit cell of m-HfO_2 as a building block, we built a spherical nanocluster with monoclinic symmetry containing 2016 classical ions and having a radius of 25 Å approximately. The coordinates of ions in this unit cell were optimized in the periodic DFT

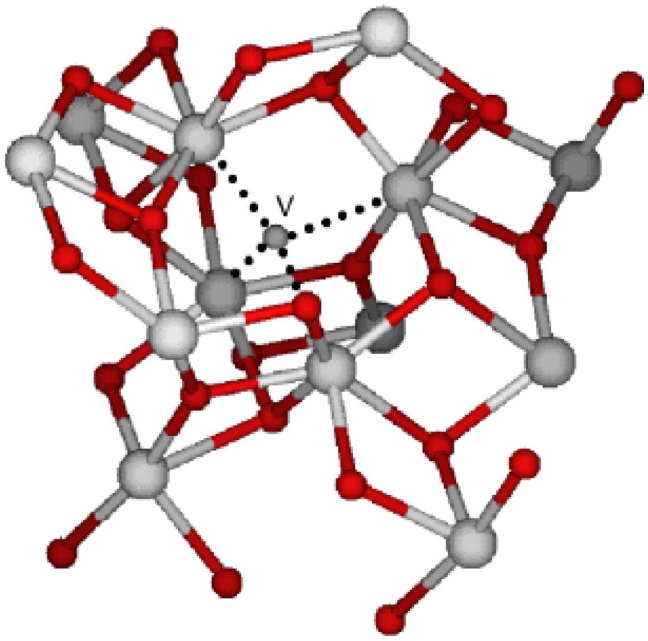

FIG. 1. (Color online) Structure of the quantum region in the embedded cluster model. Large balls correspond to Hf atoms and small balls correspond to O atoms. A small ball connected with dotted lines to nearest-neighbor Hf atoms in the center of the cluster indicates the vacancy site.

calculations using the CRYSTAL code. Then an oxygen vacancy was positioned in the center of the nanocluster. For each vacancy charge state, the positions of ions within 5 Å around the vacancy were made identical to those obtained in the periodic CRYSTAL calculations. The radius of the vacancy region was chosen to be about 5 Å, as the displacements of ions induced by the presence of the vacancy beyond this distance (calculated in the periodic model) are negligibly small. Due to the symmetry of the building blocks of this cluster, it simulates the monoclinic phase.

The ions surrounding the vacancy are treated quantum mechanically and form a so-called quantum cluster. These include 13 hafnium ions and 26 oxygen ions (25 oxygen atoms in the case of the vacancy), with the vacancy at the center of the nanocluster (see Fig. 1). All Hf ions outside the quantum cluster and within the radius of 10 Å from the vacancy were represented by large-core Hay-Wadt RECPs,[45] which substitute all but four electrons of a hafnium atom. This prevents an artificial polarization of the electron density toward positive point ions outside the quantum cluster. The point ions outside the quantum cluster carry formal charges and contribute to the electrostatic potential on the quantum cluster ions (see Ref. 46 for more details). The GTO basis sets on oxygen and hafnium ions and the pseudopotential on Hf ions in embedded cluster calculations are the same as in the periodic calculations. We also use the same B3LYP density functional.

This computational scheme is implemented in the GUESS computer code,[46] which employs the GAUSSIAN package[47] for calculating the electronic structure of the quantum cluster in the electrostatic potential of the rest of the lattice. Using this approach, we calculate the optical transition energies and

g tensor for the vacancy using the results of geometric relaxation obtained in periodic calculations.

The optical transitions were calculated using the time-dependent DFT (TDDFT) method as implemented in the GAUSSIAN98 package.[47] Although problems concerning excitations in extended systems and charge-transfer processes have been reported (see, for example, Refs. 48 and 49), in general, this method provides optical absorption spectra in good agreement with experimental data. In particular, good results have been obtained for defects in different oxides using the embedded cluster model (see, for example, Refs. 50–55). Therefore one can also expect reliable predictions of intracenter transitions for defects in hafnia. For *g*-tensor calculations, we used the technique implemented in the GAUSSIAN03 package.[56] To avoid numerical problems pertaining to using floating basis functions in this code, the basis set centered in the vacancy was not used in these calculations. Instead, an additional *d* shell was incorporated to the nearest-neighbor hafnium atoms and next-nearest-neighbor oxygen atoms to correctly describe the electron density in the vacancy. The exponents of these functions were adjusted to match the band-gap value and the defect state energies obtained with the GAUSSIAN98 calculations and have the values of 0.10 and 0.20 for Hf and O, respectively. Differences in the total energy and positions of the one-electron energy levels were less than 0.1 eV, thus verifying the compatibility of both types of calculations.

III. RESULTS

We start by discussing the electronic structure of oxygen vacancies derived from our calculations using both periodic and cluster models. We describe the results of calculations in terms of one-electron spectrum, electron density distributions, and lattice relaxation. In Sec. III B, we relate these results to the experimental measurements.

A. Electronic structure and one-electron spectrum

The single-particle band gap of m-HfO_2 obtained in our periodic calculations is 6.1 eV, which is about 0.3 eV larger than the experimental value for the optical gap[1,3] and over 2 eV larger than GGA predictions.[22,35] This one-electron energy difference neglects excitonic effects as well as phonon broadening of the band tails. These effects lead to reduction of the band gap,[57] and consideration of their influence would improve the agreement between our calculations and the experimental data.[58]

The Mulliken charges of +2.8 and −1.4 (in units of the electron charge) on the hafnium and oxygen atoms, respectively, confirm a partially ionic character of m-HfO_2. The electronic states in the valence band mainly correspond to combinations of *p* states of the oxygen atoms, although there is some small contribution of hafnium orbitals. The structure of m-HfO_2 is characterized by two types of oxygen ions coordinated by three and four Hf ions. This is reflected in the structure of the VBM: the highest occupied states, which are split from the main band by about 0.2 eV in the Γ point, are combinations of *p* orbitals of three-coordinated oxygen ions.

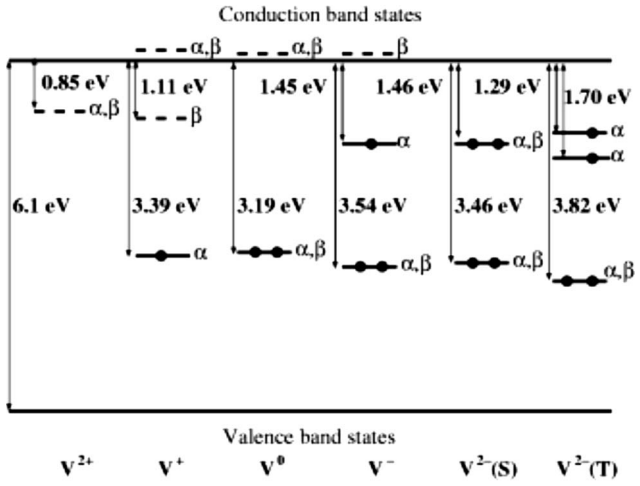

FIG. 2. One-electron level diagram for the four-coordinated oxygen vacancy in m-HfO_2 calculated using the periodic model. Continuous lines represent occupied states. Dotted lines represent unoccupied states. α and β symbols mark the spin of the state.

The electronic states in the conduction-band minimum (CBM) are formed by combinations of *d* orbitals of the hafnium ions, with some contribution of oxygen *p* states. These features are in agreement with other DFT calculations.[21,22,35,59]

Our calculations predict five possible charge states of oxygen vacancy in m-HfO_2: +2, +1, 0, −1, and −2. Neutral vacancy is formed by extracting a neutral oxygen atom from the regular site and leaving two electrons in the vacant site. Then other charge states correspond to zero, one, three, and four electrons in the vicinity of the vacancy, respectively. We will refer to these states as V^{2+}, V^{+}, V^{0}, V^{-}, and V^{2-}.

The incorporation of the vacancy does not substantially affect the band gap of the system in periodic calculations and induces a number of one-electron levels. These are shown in Fig. 2. The dispersion of single-particle energy bands corresponding to the vacancy states does not exceed 0.05 eV, reflecting the fact that the corresponding wave functions are well localized within the supercell and their overlap between periodic cells is very small. It can be seen that the presence of one or two electrons in the vacancy creates an occupied level approximately in the middle of the band gap, at 2.7 and 2.9 eV above the VBM for the +1 and 0 charged states, respectively. The isosurface of the wave function corresponding to this state at the Γ point is represented in Fig. 3(a). One can see that the middle-gap state is mostly localized in the vacancy, albeit with significant polarization toward nearest-neighbor (NN) cations. This state is composed mainly of *s* states of the vacancy basis set with small *p* and *d* contributions from the NN Hf atoms and next-NN (NNN) O atoms. The perturbation induced by the vacancy also creates a localized resonant level inside the conduction band, which is 0.2 and 0.1 eV above the CBM for V^{+} and V^{0}, respectively. This state is slightly more disperse (about 0.1 eV) than the middle-gap one. The orbital contributions to the resonant state at the Γ point can be seen in the isosurface of the wave function shown in Fig. 3(b). In this case, the symmetry of the wave function is mainly determined by a

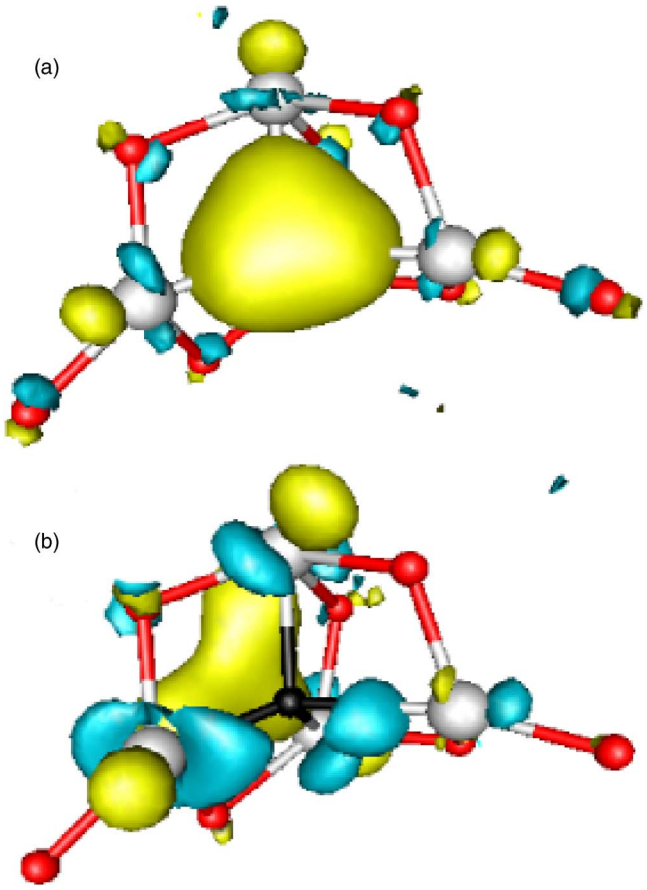

FIG. 3. (Color online) Isosurface representation of the wave function corresponding to the middle-gap one-electron level (a) and the resonant localized level (b) in the region around the vacancy in V^0. Large balls in light shade are Hf atoms and small balls in dark shade are O atoms. The position of the vacancy in this region has been represented in (b) with a dark sphere in the center of the picture.

combination of d orbitals centered on three out of four NN Hf atoms, and extended in the plane of these three ions. As one can see in Fig. 3(b), the wave function is not centered in the vacant oxygen site but rather has a maximum in a plane behind it. There are also contributions from the fourth NN Hf atom, the vacancy basis set, and the NNN O atoms, but they are smaller than the contributions of these three Hf ions.

The singly and doubly positive charged vacancies also create an unoccupied level at 0.8 and 1.1 eV (β spin) below the bottom of the conduction band, respectively, with a symmetry similar to that of the middle-gap level in V^+ and V^0, but with a smaller contribution of oxygen states. No resonant states could be detected in the conduction band for the V^{2+} vacancy. The large relaxation of the lattice in the vicinity of the vacancy in this case affects the potential well in such a way that the creation of this state is either not favored or it is so delocalized that it cannot be distinguished from the band states.

Adding one or two extra electrons to the neutral vacancy slightly lowers the energy of the doubly occupied middle-gap level and leads to the creation of additional levels below the conduction-band edge. These levels originate from the occupation of the resonant level that was located above the CBM in V^0 and V^+. In particular, in the case of V^-, the doubly occupied level is located 2.56 eV above the VBM and the singly occupied level is split 1.45 eV from the CBM, leaving an unoccupied β-spin resonant state 0.1 eV above the CBM. The α-spin state occupied by the additional electron shows less dispersion than the resonant β-spin state, indicating a strong electron localization in that single-particle state. The singlet state of the doubly negative vacancy, hereafter referred to as $V^{2-}(S)$, is 0.2 eV lower in energy than the triplet state. In this case, the middle-gap level is 2.64 eV above the VBM, while the other doubly occupied upper level is split by 1.46 eV from the CBM (see Fig. 2), leaving no resonant states in the conduction band. In the triplet state, $V^{2-}(T)$, the doubly occupied level is at 2.28 eV above the VBM, and the two singly occupied levels are split by 1.70 and 1.29 eV from the CBM. In this case, the shallower state shows a slightly larger dispersion than the 1.70 eV split state, 0.05 eV in the first case compared to 0.02 eV in the second case.

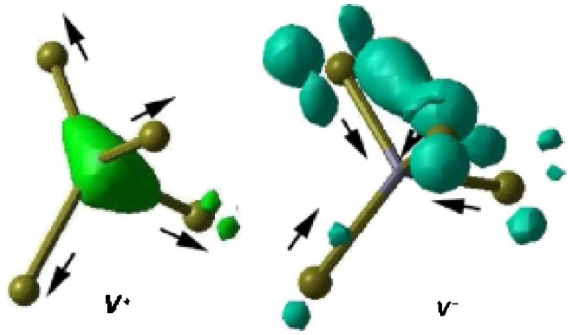

FIG. 4. (Color online) Schematic of the spin-density distribution and geometry relaxation around V^+ (left) and V^- (right) vacancies.

Different charge states are characterized by qualitatively different electron-density distributions in the vicinity of the vacancy. In the case of V^+ and V^0, the electron density is predominantly localized inside the vacancy, whereas in V^- and V^{2-}, it is mainly localized on three of the four NN Hf ions. This behavior of the density is also reflected in the lattice relaxation around the vacancy. Figure 4 shows schematically the character of the electron-density distribution and the directions of displacements of the Hf ions NN to the positively and negatively charged vacancies. The positive charge states of the vacancy are characterized by fairly symmetrical outward displacements of the NN Hf ions, on average, by about 11% and 5% of the O-Hf distance for V^{2+} and V^+, respectively. The NNN O ions displace toward the vacant site, but by a much smaller amount. This relaxation is caused by the reduced electron density in the vacancy and is characteristic of the F centers in MgO and in alkali halides (see, for example, Refs. 22 and 60). Again similar to those centers, the neutral vacancy V^0 induces almost no lattice relaxation.

In the negatively charged states, the vacancy induces the lattice distortion that decreases the NN Hf-vacancy distances. In addition, the relaxation is less symmetrical, with one of the Hf-vacancy distances less affected than the other three. The average ionic displacements in this case are about −4% for V^- and −8% for three of the hafnium centers in V^{2-}. The

fourth atom is displaced by about −5%. The oxygen ions NNN to the vacancy displace in this case outward, but these displacements are again much smaller than those for NN Hf ions. The presence of the vacancy also produces small modifications in the positions of other ions in the supercell, however, these are below 0.02 Å at distances exceeding 5 Å from the vacancy for all charge states.

The picture arising from the cluster model calculations is qualitatively very similar to that obtained in the periodic approach. This is not surprising, as the geometry around each defect state is taken from the periodic calculation, therefore producing similar perturbations in the electronic structure for both types of calculations. The valence band and conduction band are composed mainly of oxygen *p* and hafnium *d* states, respectively, similar to the periodic calculations. The value of the single-particle band gap in the nondefective embedded cluster is calculated based on the energies of highest occupied molecular orbital (HOMO) and lowest unoccupied molecular orbital (LUMO) states. In the case of the cluster with a vacancy, this difference is calculated from states which are similar to the HOMO and LUMO of the nondefective embedded cluster and have not been perturbed by the presence of the vacancy. Thus determined band gaps in the cluster and periodic calculations can be compared for both nondefective and defective systems. The band gap of the cluster representing the perfect lattice (no vacancy included) is about 0.5 eV larger than that calculated within the periodic model. The single-particle band gap of the clusters containing vacancy differs slightly from that obtained in the perfect lattice cluster, but remains in the range of 6.6–7.1 eV.

As in the case of periodic calculations, different charge states of the vacancy create one-electron levels in the band gap of the embedded cluster. Further characterization of the positions of these levels implies comparing the relative energies of one-electron levels within the same and between different embedded clusters. However, differences in the band-gap values between different vacancy charge states are not negligible, and the positions of the gap levels for different vacancy charge states are not well defined with respect to each other. The energies of the one-electron vacancy states in the gap with respect to CBM differ in periodic and embedded cluster calculations. In particular, the shallow levels of V^{2+}, V^{+}, V^{0}, and V^{-} are located deeper than in the periodic calculations by approximately 0.5–0.7 eV. In addition, the resonant defect states, analogous to those found in the periodic calculations for V^{+}, V^{0}, and V^{-}, are now the lowest energy states in the conduction band.

Thus both methods produce qualitatively similar results: deep levels in the periodic one-electron diagram remain in the lower half of the gap in the embedded cluster diagram, shallow levels stay near the conduction band, and resonant states are induced at the bottom of the conduction band. The differences in the value of the band gap and relative energies of the one-electron levels with respect to the periodic model are due to a combination of several factors: the confinement effect due to the cluster size, the small number of cluster atoms, and the perturbation created by the presence of the defect. However, there are no significant boundary effects due to the embedding procedure used in this work. We have also verified that there are no significant changes to the band gap and one-electron spectrum when the size of the quantum cluster is increased up to 50 atoms or when charges different from the formal values are assigned to the classical atoms.

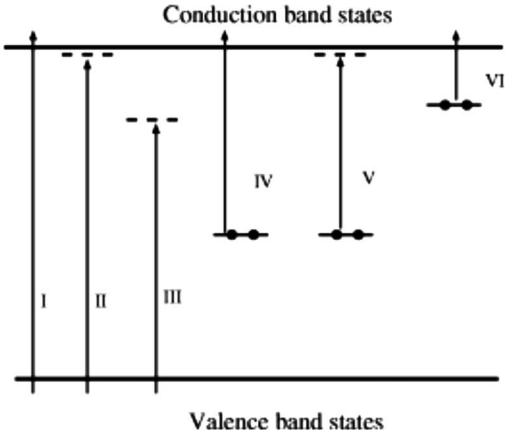

FIG. 5. Schematic of the types of optical transition present in HfO_2 with oxygen vacancy: (I) band-to-band transitions, (II) VB to resonant state transitions, (III) VB to unoccupied vacancy levels in the gap transitions, (IV) middle-gap state to CB transitions, (V) middle-gap state to resonant state transitions, and (VI) shallow-gap state to CB transitions. Note that resonant states in embedded cluster calculations are split from the CBM.

B. Spectroscopic properties

Optical absorption, optical ionization, and ESR are among the basic experimental techniques routinely used for characterizing defects in insulators. However, interpretation of these measurements is by no means straightforward even for bulk materials and can be even more difficult for ultrathin films, such as gate oxide films considered here. Recent ESR measurements[13,61] and the results of spectroscopic ellipsometry[2] provide, however, encouraging examples that such characterization is possible. The results presented below may help in identifying defects in *m*-HfO_2 films using these techniques.

1. Optical absorption energies

Optical transitions for the oxygen vacancy in different charge states were calculated using the TDDFT method and the embedded cluster model. One can distinguish six types of transitions, as illustrated in Fig. 5: (I) band-to-band transitions, (II) transitions from the valence band to resonant states in the conduction band, (III) transitions from the valence band to unoccupied vacancy levels split from the conduction band, (IV) transitions from the middle-gap occupied vacancy states to the conduction band, (V) transitions from the middle-gap occupied vacancy states to the defect-induced resonant states above the conduction-band edge, and (VI) transitions from shallow levels to the conduction band.

Table I summarizes the values of the main transitions in each charge state of the vacancy. The band-to-band transitions (type I in Fig. 5) in the perfect lattice cluster begin at 6.2 eV; these transitions have similar energies in the vacancy clusters, ranging from 6.21 eV in V^{2+} (6.59 eV in the transi-

TABLE I. The optical transition energies (in eV) with the largest oscillator strength for oxygen vacancies in m-HfO_2 involving defect gap states. The nature of each type of transition is explained in Fig. 5.

Charge	Type III	Type IV	Type V	Type VI
V^{2+}	4.94			
V^{+}	4.67	3.27	2.67	
V^{0}		3.41	2.45	
V^{-}		3.20	2.35	0.78
V^{2-}		3.25		0.92

tion with largest oscillator strength of 0.005) to 6.08 eV in $V^{2-}(S)$ (6.26 eV in the transition with largest oscillator strength of 0.005). Type II transitions, from the valence band to the resonant state in the conduction band, are present in V^{+}, V^{0}, and V^{-}. They have an energy of about 5.9 eV, with the larger oscillator strength of the order of 0.01. Type III transitions, from the valence band to the unoccupied vacancy levels split from the conduction band (see Figs. 2 and 5), are present in the V^{2+} and V^{+} cases. We have calculated 15 such transitions from the top of the valence band (VB) and from the deeper lying states. The smallest transition energies are 4.94 eV for V^{2+} and 4.68 eV for V^{+}, respectively. All transitions have small oscillator strength (maximum of 0.001 and 0.003, respectively, in the 15 calculated transitions).

Type IV transitions, from the vacancy middle-gap state toward the conduction-band states (see Figs. 2 and 5), begin at about 2.5–2.8 eV and have the maximum intensity between 3.3 and 3.4 eV, with oscillator strength between 0.08 and 0.1. This transition takes place at a state delocalized over cations in the whole cluster but having the symmetry of the defect. Therefore this relatively high oscillator strength can be an artifact of the cluster calculation. Type V transitions, from middle-gap occupied vacancy states to the resonant state in the conduction band, are present in V^{+}, V^{0}, and V^{-} centers. The lowest energy transitions have energies between 2.4 and 2.7 eV, with the oscillator strength between 0.01 and 0.04. These are among the highest in the calculated transitions, as these are transitions to a low-lying resonant state in the conduction band, with a localized character that favors high oscillator strengths.

Type VI transitions, from occupied vacancy levels near the CBM to conduction-band states, are present in the negatively charged vacancy clusters. These transitions begin at low energies: 0.78–0.90 eV for V^{-} and 0.92 eV for $V^{2-}(S)$, and have small oscillator strength of the order of 0.005.

Calculated transitions from the valence band to the unoccupied defect states of V^{2+} and V^{+} (β spin) (type III) are in the range of 4.5–5.0 eV, which are consistent with the reflection ellipsometry data by Takeuchi *et al.*[2]

We note that the method of calculation and the presence of resonant states in the one-electron spectrum strongly affects the absorption spectrum. For example, in the case of V^{+}, the transition energy from the deep level to the conduction band calculated through one-electron energy differences is 4.22 eV. This value becomes 3.71 eV if a resonant state is taken instead, which is 0.5 eV less than the previous result. Now if we compare these numbers with the TDDFT values calculated for the latter transition (Table I), there is almost 1 eV difference between the two methods. This demonstrates that one-electron level differences provide poor estimate of optical transition energies.

2. ESR properties

Using the embedded cluster method, we have also calculated the g tensor for V^{+} and V^{-} vacancies which contain an unpaired electron. The principal values for V^{+} are 1.9450, 1.9630, and 1.9835, whereas for V^{-}, these values are 1.8108, 1.8448, and 1.9410. Unlike negative vacancies, positive oxygen vacancies are more stable in three-coordinated rather than four-coordinated sites. Therefore we carried out g-tensor calculation also for a three-coordinated V^{+} vacancy. The geometric configuration of the vacancy was obtained, in the same way as before, from a CRYSTAL periodic calculation. The distribution of one-electron levels in the cluster model is similar to that obtained for the four-coordinated case, with a band gap of 7.2 eV and defect levels higher in the gap by about 0.3 eV. The principal values of g tensor obtained in this case are 1.927, 1.938, and 1.960. Although, the symmetry of g tensor is orthorhombic, the g_{xx} and g_{yy} components have much closer values than in the four-coordinated case due to the approximately trigonal planar symmetry of the three-coordinated vacancy.

Several experimental works[13,61] observed ESR signals after irradiation or electron treatment of m-HfO_2 films, with two well differentiated signals: one whose principal g values provide strong evidence that it is due to O_2^- and another for which they obtained a zero crossing value of 1.96. More recently, Wright and Barklie[14] were able to obtain the principal values for this particular signal from measurements on m-HfO_2 powders, with $g_{\parallel}=1.940(3)$ and $g_{\perp}=1.970(2)$. This signal has been tentatively attributed in these works to a Hf^{3+} related ion defect, although contributions from other d^1 impurities in the sample like Ti^{3+} or charged oxygen vacancies have also been considered. Comparison of these data with our calculated values for the V^{+} and V^{-} oxygen vacancies provides some useful information toward the identification of this signal. First, the electron-density distribution in V^{-} can be interpreted as a combination of a neutral vacancy NN to a Hf^{3+} ion, as the third electron of V^{-} is localized in some of the NN Hf atoms, one of them accumulating more spin density than the others. The principal values for the g tensor of this defect are very different from the experimental value, suggesting that Hf^{3+} is not a good candidate for this signal. On the other hand, the g values obtained for V^{+}, specially in the three-coordinated site, are in better agreement with the experimental g value. The main discrepancy in this case is the symmetry of the g tensor. The experimental value shows an axial symmetry, while in our calculations, the three principal values are appreciably different, although the g_{xx} and g_{yy} components present values closer to each other than to the g_{zz} component. Study of the correlation of optical absorption data with this ESR signal could contribute in clarifying the identity of the defect responsible for the ESR activity.

3. Optical and thermal ionization energies

Optical absorption and ESR do not exhaust all experimental techniques which can be used to probe defect properties

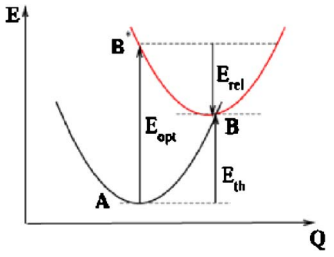

FIG. 6. (Color online) Energy diagram for the detrapping process.

in HfO_2. Another common type of experiment concerns measuring the onset of photoinduced current, which is related to optical ionization of defect states into the conduction band, and characteristics of devices under electrical stress. In particular, Bersuker *et al.*[16] measured changes of the threshold voltage of a MOSFET with *m*-HfO_2 as a gate dielectric under electrical stress at different temperatures. The kinetics of such voltage variations points at the existence of thermally activated processes with two characteristic energies, 0.35 and 0.5 eV. These processes were interpreted as thermally activated escape of electrons from shallow electron traps into the conduction band of HfO_2.

Optical and thermal ionizations of vacancies to the bottom of the conduction band result from different processes, as illustrated in Fig. 6. The system is initially in the state A. In optical ionization process obeying the Frank-Condon principle, the nuclei of the ions do not respond to the electron excitation event immediately and therefore it takes place vertically; i.e., in the final ionized state (state B^* in Fig. 6), the nuclei remain initially in the same positions as in the initial state. Then the system undergoes relaxation into the minimum of the ionized state (state B). Thermal ionization process, on the other hand, requires that the system is thermally excited to the crossing point of the initial, A, and final, B, states. Our calculations show that this crossing point for ionization of negatively charged vacancies is located close to the minimum of the ionized state (see Fig. 6). Therefore the thermal ionization energy is effectively smaller than the optical ionization energy by the amount of the lattice relaxation energy in the ionized state. This approximate relation can be expressed as

$$E_{th}(q) = E_{opt}(q) - E_{rel}(q), \tag{1}$$

where $E_{th}(q)$ refers to the thermal ionization energy of the vacancy in the charge state q, $E_{opt}(q)$ refers to the optical ionization energy, and $E_{rel}(q)$ refers to the relaxation energy.

Optical ionization energies can be calculated using two different methods. In the first method, one assumes that the excited state of system B^* corresponds to the ionized electron at the bottom of the conduction band far away from the ionized defect so that they do not interact. The second method takes into account the defect-induced perturbation of the crystal and the interaction between the ionized defect and the electron in the excited state B^*. The latter process is closer to reality and can be simulated in the embedded cluster model as optical transition types IV–VI with the largest oscillator strength. Note that these transitions take place not necessarily at the bottom of the conduction band. The system then relaxes to the state with the free electron at the bottom of the conduction band.

TABLE II. Optical excitation energies E_{opt}, relaxation energies E_{rel}, and thermal activation energies E_{th} for oxygen vacancies in *m*-HfO_2, calculated according to Eqs. (1)–(3).

q	E_{opt}	E_{rel}	E_{th}
V^+	3.33	1.01	2.32
V^0	3.13	0.80	2.33
V^-	1.24	0.48	0.76
V^{2-}	0.99	0.43	0.56

The ionization energies corresponding to the first method are easier to calculate: they can be deduced from the total energies of different systems calculated in the periodic model as follows:

$$E_{opt}(V^q) = E_q(V^{q+1}) - E_q(V^q) + E^- - E^0, \tag{2}$$

where E^0 is the total energy of the perfect HfO_2 crystal, and E^- corresponds to the total energy of the perfect HfO_2 crystal with an electron at the bottom of the conduction band. $E_q(V^q)$ is the total energy of the system with the vacancy in a charge state q ($q=+2$, $+1$, 0, -1, and -2) in the optimized geometry, and $E_q(V^{q+1})$ is the total energy of the vacancy in the charge state $q+1$ but at the equilibrium geometry corresponding to the vacancy in the charge state q. The relaxation energy (E_{rel}) associated with this process can be calculated as

$$E_{rel}(V^{q+1}) = E_{q+1}(V^{q+1}) - E_q(V^{q+1}). \tag{3}$$

We note that the above considerations assume that the vacancy is far away from the interface and only the bulk properties of HfO_2 are involved in these energies, otherwise Si or metal band alignment should be taken into account.

The values of E_{opt}, E_{rel}, and E_{th} for different charge states of the vacancy calculated using the first method and the periodic model are summarized in Table II. Interestingly, E_{rel} for the negatively charged vacancy is smaller than that for the positively charged vacancy. Direct numerical comparison of these optical ionization energies with the results obtained in the embedded cluster model using TDDFT is hampered by the difference in the band-gap energies and positions of defect levels in both models. Semiquantitatively, however, the obtained ionization values are quite similar and differ only within 0.5 eV. We also note that optical ionization energies E_{opt} calculated as total energy differences and Eq. (2) are close to single-electron energy differences. This is in line with the Janak theorem, which relates the total energy differences for the systems with N and $N\pm1$ electrons in DFT calculations to the single-particle energies of the HOMO and LUMO.

The thermal ionization energies E_{th} are 0.5–1.0 eV smaller than the optical energies due to the large lattice relaxation associated with the change of the charge state of the vacancy. In particular, although the single-particle energies

for the V^- and V^{2-} are very similar, thermal ionization energies of these defects differ by 0.2 eV. The obtained thermal ionization energies are qualitatively consistent with the energies 0.35 and 0.5 eV extracted by Bersuker *et al.* Very large detrapping energies for the V^+ and V^0 vacancies rule out these species as possible shallow electron traps. We should note that thermal broadening of the defect levels and band tails, which is not taken into account in our calculations, would improve the agreement between the calculated thermal ionization energies and the experimental energies even further.

Finally, we note that energy diagrams like the one shown in Fig. 2 are often used to predict the population of defect states due to tunneling from the substrate material, e.g., Si. Neglecting the interface band bending as above, one can make such a prediction using total energies and the theory described in Ref. 62. Using the same approach as described above, it is easy to show that predictions regarding possible occupation of a vacancy in the charge state $q+1$ by an extra electron tunneling from Si can be made by comparing the optical ionization energy of the vacancy in the charge state q to the bottom of the conduction band with the band offset of the top of the Si valence band with respect to the conduction band of HfO_2 (note that we are using the same reference energy and the same type of optical measurement here). If $E_{opt}(V^q)$ is greater than the band offset energy, the resonant tunneling into V^{q+1} vacancy will be exothermic and the energy equal to the difference between the two numbers will be released as phonons. If this difference is negative but small, tunneling can be thermally activated and/or stimulated by bias application. We can compare energies given in Table II with the experimental band offset energies measured using internal photoemission in Refs. 63 and 64. These measurements predict the band gap of 5.6 eV and the band offset between the top of the Si valence band and the bottom of the HfO_2 conduction band of 3.1 eV. The latter value is slightly smaller than E_{opt} for both single positively charged and neutral vacancies. This indicates that in flatband conditions, electrons can tunnel into double and single positively charged vacancy states. Since our calculated band gap is 6.1 eV, we hold this as a reliable qualitative prediction. Neutral and single negatively charged states can trap extra electrons through hot electron injection from Si.

IV. DISCUSSION AND CONCLUSIONS

To summarize, we have calculated the positions of single-electron levels for five charge states of oxygen vacancy in m-HfO_2 using periodic and embedded cluster DFT methods and related them to spectroscopic defect properties, which can be measured using common experimental techniques. The results of trap recharging measurements are consistent with thermal ionization of negatively charged V^- and V^{2-} centers, whereas the spectroscopic ellipsometry data can be interpreted as optical excitation of positively charged V^+ or V^{2+} vacancies. The calculated g tensor for the V^+ and V^- centers may help their experimental identification.

Given the multitude of charge states of oxygen vacancy, it is important to understand which vacancy charge states dominate in the stack with and without gate bias. To this end, let us consider a device with a n-Si channel. Let us assume that initially all the vacancies are fully ionized (i.e., the predominant vacancy state is V^{2+}). The corresponding virtual energy level is substantially above the CBM of Si and, thus, above the global Fermi level of the system. This is the first equilibrium state. Applying positive bias to the gate may lead to electron transfer from the Si channel into vacancies. If the bias pulse is sufficiently long and the concentration of vacancies is low (the interaction between the vacancies is weak), all of them can eventually trap up to four electrons (V^{2-} state). After the gate bias is returned to zero, all the charge states with energies above the Fermi level will eventually disappear. However, the kinetics of this process is determined by the limited number of vacancy ionization mechanisms. So, although V^{2-} states are thermodynamically unstable, they may be sufficiently long lived. Being nonequilibrium, all the V^{2-} and V^- states will eventually ionize, evolving to V^0 states whose relaxed energy is near Si midgap and, thus, below the global Fermi level. Therefore V^0 states represent another thermodynamic equilibrium as at zero bias electrons from V^0 states will not escape. Therefore, in order to fully ionize vacancies into their initial state V^{2+}, a negative gate bias should be applied. This is consistent with experimental observations on detrapping.[18] Thus stable charge states of the vacancy are V^0 and V^{2+}, depending on the number of electrons in the system. However, other charge states can also be important at nonequilibrium conditions.

The existence of two stable negatively charge states of the oxygen vacancy in this system is a remarkable feature, as double negatively charged oxygen vacancies are not commonly reported in oxides. The best studied defect of this type in wide-gap insulators is a so-called F′ center in alkali halides, where a vacancy of a halide ion accommodates two extra electrons.[65] Therefore it is negatively charged, but both electrons occupy the same s-like ground state of the vacancy. In the case of HfO_2, the extra electron(s) in a negatively charged vacancy occupies the higher-lying state in the potential well created by the vacancy.

There have been several attempts in the past to use simple models for predicting energy levels of an electron trapped in an anion vacancy (see, for example, Refs. 66 and 67). In particular, a spherically symmetric potential well of finite depth (SSPFD) model has been used quite successfully to predict a number of bound states in an F center in a range of alkali halides.[67] A more complex well model has been discussed in Ref. 66. In the SSPFD model, the number of levels is determined by the well strength, which is a product of the well depth and the square of the well radius: roughly, a deeper and narrower well can accommodate more levels.[67] To check whether this simple model can be useful for understanding the results of our calculations, we calculated the one-electron spectrum of V^{2+} center in the geometry of the less distorted V^+ center. We have also carried out a calculation of V^+ in a more distorted environment, corresponding to the geometry of the fully relaxed V^{2+} vacancy. We observed that in the case of V^{2+} with geometry of V^+, a level with the symmetry of the resonant levels in V^+ and V^0 splits from the conduction band. In addition, the calculation of V^+ with the geometry of V^{2+} reveals that the resonant level obtained in

the fully relaxed geometry is missing in this setup. These calculations suggest that the lattice distortion induced by V^{2+} may be responsible for the nonexistence of the resonant level. If this simple model is right, the ability of the oxygen vacancy to trap up to two extra electrons can be due to the high dielectric constant of HfO_2, whereby the electron-induced polarization of the lattice makes the well deeper through a polaron effect, whereas the inward displacements of the nearest Hf ions make the well narrower.

In more general terms, this study is representative of a much broader effort to establish the properties of defects in other gate oxide materials and is one of the early attempts to link the one-electron defect properties to the experimental data. As was mentioned in Sec. I, there have been numerous calculations of the oxygen vacancy in different phases of zirconia and hafnia over the last 15 years or so. Several early studies used plane-wave DFT methods and local functionals[35,68,69] and suffered from the underestimated band-gap problem. Very recent studies employed the most advanced methods including GW, screened exchange, and weighted density approximations.[28,29,59,70] These latter calculations as well as the periodic calculations using the nonlocal exchange density functionals presented here are very computationally expensive. The net result of these periodic calculations is the relative stability of different defect charge states and positions of the one-electron defect levels in the band gap of the oxide. Thinking about future work on testing other potential gate oxide candidates, the issue of the accuracy of relatively cheap plane-wave DFT calculations with local functionals in predicting defect charge states and positions of one-electron defect levels is worth contemplating.

To address this question, one can compare the results of the oxygen vacancy calculations by different methods. For example, LDA and GGA calculations underestimate the band gap of m-HfO_2 by approximately 2 eV (Refs. 26, 35, 68, and 69) (see Fig. 7). Our GGA calculations[26] predicted the existence of all five vacancy charge states, but the one-electron levels of negatively charged vacancies were very close to the CBM, as can be seen in Fig. 7. A common method of overcoming this problem and more accurately determining the positions of defect levels in the gap is to use the so-called scissor operator.[35,71] The simplified procedure consists of moving the energy of the unoccupied bands to match the experimental gap values. This leads to the problem of deciding how to move the levels induced by the vacancy, to which several solutions have been proposed. Foster *et al.*[35] linked the defect levels to the valence band, thus moving only the states above the bottom of the conduction band. They found the positions of the V^0 and V^+ states at 2.3 and 1.6 eV, respectively, above the VBM. These values compare reasonably well with the B3LYP values, taking into account the different band gaps in both types of functional. On the other hand, this procedure predicts splitting of the unoccupied level of V^{2+} from the CBM of 2.93 eV, much greater than the value of 0.8 eV obtained in the B3LYP calculations. Another possibility is to move the vacancy levels together with the conduction band; this way one obtains the one-electron levels much higher in the gap than in B3LYP calculations, except again in the case of V^{2+}.

Now, if we look at the case of V^- and V^{2-}, we see that pinning these levels to the VBM leads to a splitting from the

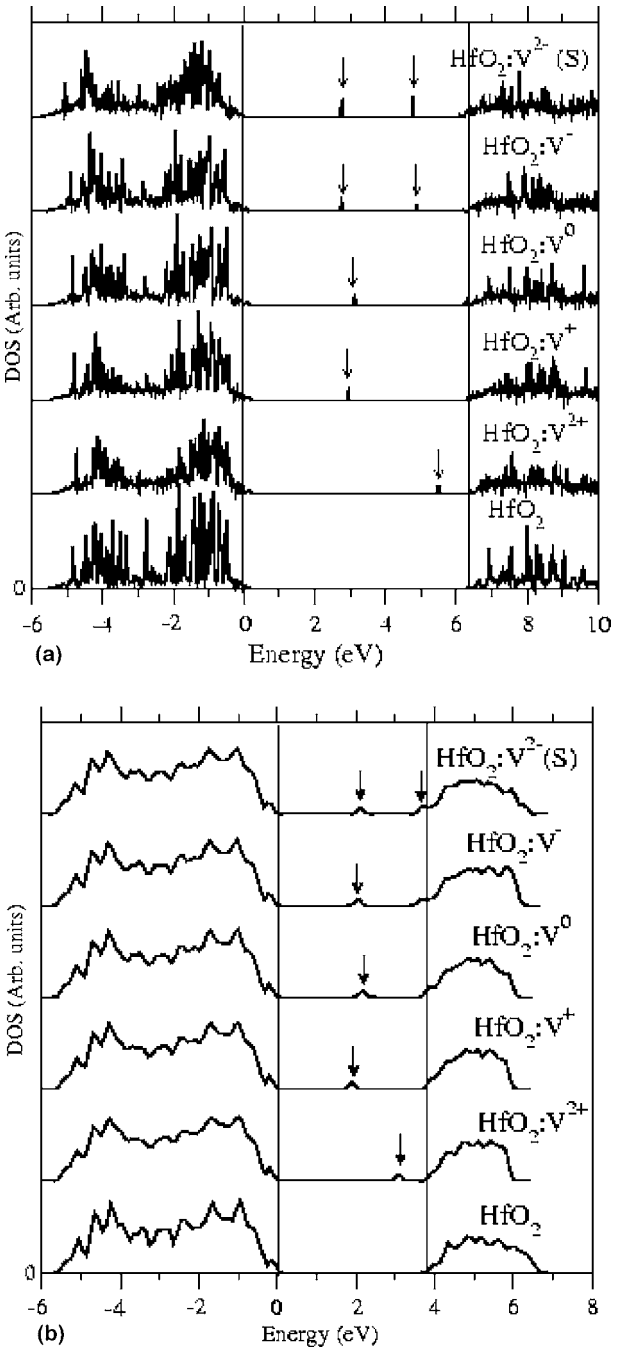

FIG. 7. Density of states in the gap region of HfO_2 with a four-coordinated oxygen vacancy in different charge states calculated with (a) the B3LYP and (b) the GGA functionals.

CBM of about 1.5 eV, while pinning them to the CBM results in a splitting of under 0.1 eV. One can infer from this comparison with the B3LYP results that in LDA and/or GGA, only deep occupied one-electron levels are reasonably well represented. We note also that this procedure is based on the assumption that the error in the position of the conduction band is much larger than that in the position of the valence band, and that the last one is negligible. The accuracy of this assumption, in general, is hard to justify.

Some other methods give good estimates of the band gap, but most of the calculations have been performed in the cu-

TABLE III. Comparison of band-gap energies and defect level splittings (in eV) obtained using different theoretical methods. Energies of defect levels are calculated with respect to the CBM (see Fig. 2). For V^{2+} center, the position of the unoccupied level is shown. For V^{+} center, the position of the single occupied level is shown. For V^{-} and V^{2-}, the positions of both deep and shallow levels are shown.

Method	GGA[a]	sX[b]	B3LYP
Gap	4.2	5.5	6.1
V^{2+}	0.5	0.3	0.8
V^{+}	2.6	0.8	3.4
V^{0}	1.9	1.7	3.2
V^{-}	2.1, 0.1	1.7, 0.5	3.5, 1.5
V^{2-}	2.1, 0.1	1.7, 0.25	3.5, 1.5

[a]Reference 26.
[b]Reference 29.

bic phase. Nevertheless, the band gap should be similar to that in the monoclinic phase. In particular, Kralik *et al.*[59] report GW calculations of the neutral vacancy in cubic ZrO_2. An indirect band gap of 5.6 eV has been predicted, with the V^0 level 2.1 eV below the CBM. Our B3LYP calculations for the identical system (neutral vacancy in the 12-atom cubic supercell) give similar predictions of an indirect gap of 5.3 eV and a position of the V^0 level 2.5 eV below the CBM. Xiong *et al.*[28,29,70] used the sX method in a GGA-relaxed supercell and obtained a band gap of 5.75 eV. However, these calculations predict vacancy one-electron energies higher in the gap than those predicted by B3LYP (see Table III). The origin of this difference is not yet clear. One of the reasons could be that these methods do not fully include the lattice relaxation. The calculations have been performed either in the ideal cell or using the defect geometry obtained within GGA. In our B3LYP calculations, the defect geometry is obtained consistently within the same method. Supercell size can also be an important factor; the 96-atom supercell considered in our calculations doubles the size of the supercells used in the other calculations. Another reason could be much deeper and could relate to the details of implementation of exchange and correlation functionals in these different methods. This issue requires detailed investigation, which should be possible with further increase of computer power and development of more accurate techniques for calculating spectroscopic properties.

Finally, we note that, although prediction of negative oxygen vacancy states brings more consistency between theory and optical and electrical measurements, it does not prove that such vacancies present the only shallow electron traps, or even that they are universally dominant traps. Alternative possibilities such as polaronic traps[72] or impurity metals[26] are also being considered. Careful experiments with films with controlled vacancy concentration should help to resolve this issue.

Note added in proof. Recently, another study on HfO_2 oxygen vacancies has been published with qualitatively similar results.[73]

ACKNOWLEDGMENTS

The authors would like to thank V. Afanas'ev, A. Stesmans, J. Robertson, and I. Abarenkov for valuable discussions. The authors are grateful to P. Sushko for help in setting up embedded cluster calculations and valuable discussions. D.M.R. and J.L.G. were supported by EPSRC Grant No. GR/S80080/01. The computer time on the HPCx facility was awarded to the Materials Chemistry consortium under EPSRC Grant No. GR/S13422/01 "Materials Chemistry using Teraflop Computing."

[1] M. Houssa, in *High-k Dielectrics*, edited by M. Houssa (IOP, Bristol, 2004), p. 597.
[2] H. Takeuchi, D. Ha, and T.-K. King, J. Vac. Sci. Technol. A **22**, 1337 (2004).
[3] N. V. Nguyen, A. V. Davydov, D. Chandler-Horowitz, and M. M. Frank, Appl. Phys. Lett. **87**, 192903 (2005).
[4] The experiments by Nguyen *et al.* were conducted in vacuum ultraviolet region, so it is not clear whether the absorption energy region below 5 eV was scanned.
[5] A. Stesmans and V. V. Afanas'ev, Appl. Phys. Lett. **82**, 4074 (2003).
[6] A. Stesmans and V. Afanas'ev, in *Defects in Advanced High-k Dielectric Nano-Electronic Semiconductor Devices*, edited by E. Gusev (Springer, New York, 2006), pp. 215–226.
[7] A. Kang, P. M. Lenahan, J. F. Conley, Jr., and R. Solanki, Appl. Phys. Lett. **81**, 1128 (2002).
[8] P. M. Lenahan and J. F. Conley, Jr., IEEE Trans. Device Mater. Reliab. **5**, 90 (2005).
[9] T. G. Privicko, J. P. Campbell, P. M. Lenahan, W. Tsai, and A. Kerber, Appl. Phys. Lett. **86**, 173511 (2005).
[10] P. M. Lenahan and J. F. Conley, Jr., J. Vac. Sci. Technol. B **16**, 2134 (1998).
[11] P. M. Lenahan and P. V. Dressendorfer, J. Appl. Phys. **55**, 3495 (1984).
[12] G. Bersuker, C. S. Park, J. Barnett, P. S. Lysaght, P. D. Kirsch, C. D. Young, R. Choi, B. H. Lee, B. Foran, K. van Benthem, S. J. Pennycook, P. M. Lenahan, and J. T. Ryan, J. Appl. Phys. **100**, 094108 (2006).
[13] A. Y. Kang, P. M. Lenahan, and J. Conley, Jr., Appl. Phys. Lett. **83**, 3407 (2003).
[14] S. Wright and R. C. Barklie, Mater. Sci. Semicond. Process. **9**, 892 (2006).
[15] G. Bersuker, J. H. Sim, C. D. Young, C. S. Park, R. Choi, P. M. Zeitzoff, G. A. Brown, B. H. Lee, and R. Murto, Microelectron. Reliab. **44**, 1509 (2004).
[16] G. Bersuker, J. Sim, C. S. Park, C. Young, S. Nadkarni, R. Choi, and B. H. Lee, IEEE Int. Reliab. Phys. Symp. Proc. **44**, 179 (2006); and (to be published).
[17] G. Ribes, J. Mitard, M. Denais, S. Bruyere, F. Monsieur, C. Parthasarathy, E. Vincent, and G. Ghibaudo, IEEE Trans. Device

Mater. Reliab. **5**, 5 (2005).
[18] J. Mitard, C. Leroux, G. Reimbold, X. Garros, F. Martin, and G. Ghibaudo, in *Defects in Advanced High-k Dielectric Nano-Electronic Semiconductor Devices*, edited by E. Gusev (Springer, New York, 2006), pp. 85–96.
[19] G. Bersuker, P. Zeitzoff, J. Sim, B. Lee, R. Choi, G. Brown, and C. D. Young, Appl. Phys. Lett. **87**, 042905 (2005).
[20] J. L. Gavartin, D. Muñoz Ramo, A. L. Shluger, G. Bersuker, and B. H. Lee, Appl. Phys. Lett. **89**, 082908 (2006).
[21] J. Robertson, Rep. Prog. Phys. **69**, 327 (2006).
[22] A. L. Shluger, A. S. Foster, J. L. Gavartin, and P. V. Sushko, in *In Nano and Giga Challenges in Microelectronics*, edited by J. Greer, A. Korkin, and J. Labanowski (Elsevier, New York, 2003), pp. 151–222.
[23] J. Gavartin, A. S. Foster, G. I. Bersuker, and A. L. Shluger, J. Appl. Phys. **97**, 053704 (2005).
[24] C. G. Van de Walle, J. Appl. Phys. **95**, 3851 (2004).
[25] C. Shen, M. F. Li, X. P. Wang, H. Y. Yu, Y. P. Feng, A. T. L. Lim, Y. C. Yeo, D. S. H. Chan, and D. L. Kwong, Tech. Dig. - Int. Electron Devices Meet. **2004**, 733.
[26] G. Bersuker, B. Lee, H. Huff, J. Gavartin, and A. Shluger, in *Defects in Advanced High-k Dielectric Nano-Electronic Semiconductor Devices*, edited by E. Gusev (Springer, New York, 2006), pp. 227–236.
[27] K. Xiong and J. Robertson, Microelectron. Eng. **80**, 408 (2005).
[28] K. Xiong, J. Robertson, M. C. Gibson, and S. G. Clark, Appl. Phys. Lett. **87**, 183505 (2005).
[29] K. Xiong, J. Robertson, and S. J. Clark, Phys. Status Solidi B **243**, 2071 (2006).
[30] V. Saunders, R. Dovesi, C. Roetti, R. Orlando, C. M. Zicovich-Wilson, N. M. Harrison, K. Doll, B. Civalleri, B. Bush, and P. L. M. D'Arco, *CRYSTAL 2003 User's Manual* (University of Torino, Torino, 2003).
[31] R. Dovesi, B. Civalleri, R. Orlando, C. Roetti, and V. R. Saunders, Rev. Comput. Chem. **21**, 1 (2005).
[32] F. Cora, M. Alfredsson, G. Mallia, D. S. Middlemiss, W. C. Mackrodt, R. Dovesi, and R. Orlando, Struct. Bonding (Berlin) **113**, 171 (2004).
[33] M. D. Towler, N. L. Allan, N. M. Harrison, V. R. Saunders, W. C. Mackrodt, and E. Apra, Phys. Rev. B **50**, 5041 (1994).
[34] W. J. Stevens, M. Krauss, H. Basch, and P. G. Jasien, Can. J. Chem. **70**, 612 (1992).
[35] A. S. Foster, F. Lopez Gejo, A. L. Shluger, and R. M. Nieminen, Phys. Rev. B **65**, 174117 (2002).
[36] A. D. Becke, J. Chem. Phys. **98**, 5648 (1993).
[37] C. Lee, W. Yang, and R. G. Parr, Phys. Rev. B **37**, 785 (1988).
[38] A. Wander, I. J. Bush, and N. M. Harrison, Phys. Rev. B **68**, 233405 (2003).
[39] A. Wander and N. M. Harrison, Surf. Sci. **457**, L342 (2000).
[40] J. R. B. Gomes, I. D. R. Moreira, P. Reinhardt, A. Wander, B. G. Searle, N. M. Harrison, and F. Illas, Chem. Phys. Lett. **341**, 412 (2001).
[41] J. Muscat, A. Wander, and N. M. Harrison, Chem. Phys. Lett. **342**, 397 (2001).
[42] V. B. Sulimov, P. V. Sushko, A. H. Edwards, A. L. Shluger, and A. M. Stoneham, Phys. Rev. B **66**, 024108 (2002).
[43] H. Lin, Y. Zhao, O. Tishchenko, and D. G. Truhlar, J. Chem. Theory Comput. **2**, 1237 (2006).
[44] A. A. Sokol, S. T. Bromley, S. A. French, C. R. A. Catlow, and P. Sherwood, Int. J. Quantum Chem. **99**, 695 (2004).
[45] P. J. Hay and W. R. Wadt, J. Chem. Phys. **82**, 270 (1985).
[46] P. V. Sushko, A. L. Shluger, and C. R. A. Catlow, Surf. Sci. **450**, 153 (2000).
[47] M. J. Frisch *et al.*, GAUSSIAN 98, Revision A7, Gaussian, Inc., Pittsburgh, PA, 1998.
[48] L. Serrano-Andrés and M. Merchán, J. Mol. Struct.: THEOCHEM **729**, 99 (2005).
[49] G. Onida, L. Reining, and A. Rubio, Rev. Mod. Phys. **74**, 601 (2002).
[50] S. Mukhopadhyay, P. V. Sushko, A. M. Stoneham, and A. L. Shluger, Phys. Rev. B **71**, 235204 (2005).
[51] P. V. Sushko, S. Mukhopadhyay, A. M. Stoneham, and A. L. Shluger, Microelectron. Eng. **80**, 292 (2005).
[52] S. Mukhopadhyay, P. V. Sushko, V. A. Mashkov, and A. L. Shluger, J. Phys.: Condens. Matter **17**, 1311 (2005).
[53] P. V. Sushko, S. Mukhopadhyay, A. S. Mysovsky, V. B. Sulimov, A. Taga, and A. L. Shluger, J. Phys.: Condens. Matter **17**, S2115 (2005).
[54] J. Carrasco, C. Sousa, F. Illas, P. V. Sushko, and A. L. Shluger, J. Chem. Phys. **125**, 074710 (2006).
[55] M. Miyakawa, H. Kamioka, M. Hirano, T. Kamiya, P. V. Sushko, A. L. Shluger, N. Matsunami, and H. Hosono, Phys. Rev. B **73**, 205108 (2006).
[56] M. J. Frisch *et al.*, GAUSSIAN 03, Revision C02, Gaussian, Inc., Wallingford, CT, 2003.
[57] S. Sayan, T. Emge, E. Garfunkel, X. Zhao, L. Wielunski, D. Vanderbilt, J. S. Suehle, S. Suzer, and M. Banaszak-Holl, J. Appl. Phys. **96**, 7485 (2004).
[58] V. V. Afanas'ev, A. Stesmans, F. Chen, X. Shi, and S. A. Campbell, Appl. Phys. Lett. **81**, 1053 (2002).
[59] B. Kralik, E. K. Chang, and S. G. Louie, Phys. Rev. B **57**, 7027 (1998).
[60] J. Carrasco, N. Lopez, and F. Illas, J. Chem. Phys. **122**, 224705 (2005).
[61] J. T. Ryan, P. M. Lenahan, A. Y. Kang, J. F. Conley, Jr., G. Bersuker, and P. Lysaght, IEEE Trans. Nucl. Sci. **52**, 2272 (2005).
[62] W. B. Fowler, J. K. Rudra, M. E. Zvanut, and F. J. Feigl, Phys. Rev. B **41**, 8313 (1990).
[63] V. V. Afanas'ev, A. Stesmans, C. Zhao, M. Caymax, T. Heeg, J. Schubert, Y. Jia, D. G. Schlom, and G. Lucovsky, Appl. Phys. Lett. **85**, 5917 (2004).
[64] V. V. Afanas'ev and A. Stesmans, in *High-k Dielectrics*, edited by M. Houssa (IOP, Bristol, 2004), pp. 217–250.
[65] M. Georgiev, *F′ Centers in Alkali Halides*, Lecture Notes in Physics (Springer, Berlin, 1989).
[66] J. A. Krumhansl and N. Schwartz, Phys. Rev. **89**, 1154 (1953).
[67] Z. S. Herman and G. Barnett, Rev. Bras. Fis. **12**, 73 (1982).
[68] A. S. Foster, V. B. Sulimov, F. Lopez Gejo, A. L. Shluger, and R. M. Nieminen, Phys. Rev. B **64**, 224108 (2001).
[69] J. Kang, E. C. Lee, K. J. Chang, and Y. G. Jin, Appl. Phys. Lett. **84**, 3894 (2004).
[70] J. Robertson, K. Xiong, and S. J. Clark, Phys. Status Solidi B **243**, 2054 (2006).
[71] V. Fiorentini and A. Baldereschi, J. Phys.: Condens. Matter **4**, 5967 (1992).
[72] J. L. Gavartin, D. Muñoz Ramo, A. L. Shluger, and G. Bersuker, ECS. Trans. **3**, 277 (2006).
[73] P. Broqvist and A. Pasquarello, Appl. Phys. Lett. **89**, 262904 (2006).